OMAR FADHIL ABDULLAH[1]
ORCID: 0000-0002-3040-0000
E-mail: omarmaterials@uosamarra.edu.iq

ORASS ABDULHADI HUSSEIN[1]
ORCID: 0000-0002-5260-985X
E-mail: orass84@yahoo.com

MARWAN AL-LATTOUF[1]
ORCID: 0009-0002-1209-1133
E-mail: marwan.ka.abd@uosamarra.edu.iq

SALIH Y. DARWEESH[2,*]
ORCID: 0000-0002-4207-4177
E-mail: salih.younis@tu.edu.iq

[1] Physics Department, College of Education, Samarra University, Samarra, Iraq
[2] Physics Department, College of Science, Tikrit University, Tikrit, Iraq
* Corresponding author

DOI: 10.15199/40.2024.11.2

Effect of laser surface treatment on properties of S-Monel alloy nanoparticles fabricated via powder technology

Wpływ laserowej obróbki powierzchni na właściwości nanocząstek stopu S-Monel wytworzonych w technologii proszkowej

This study aimed to fabricate S-Monel alloy (66% Ni, 30% Cu, 4% Si) using powder technology for its technological and economic worth. After tacking, silicon, copper, and nickel powders were combined in the ratios mentioned above and crushed under isostatic cold pressure (8 t). At a distance of 100 cm, the samples underwent laser surface treatment with varying energies (0 mJ, 200 mJ, 260 mJ, and 300 mJ) and pulse durations (10 s). The X-ray diffraction test indicated that all samples have a face-centered cubic (FCC) structure. Notably, the samples treated with 300 mJ exhibited the best properties, including an increase in phase intensity. The laser treatment melted all surface molecules, resulting in improved structural characteristics. Hardness value (Rockwell method), apparent density, water absorption, and porosity were all impacted by surface laser treatment. On the other hand, samples were immersed in a 3.5% NaCl solution for 3, 5, 7, 9, and 11 days to examine the impact of heat treatment on alloy corrosion resistance. Hardness parameters increased while the porosity ratio and water absorption reduced after laser treatment. It has also been found that wear resistance increases with increased laser therapy.

Keywords: laser treatment, XRD, Monel alloy, powder technology

Przedmiotem badań było wytworzenie stopu S-Monel (66% Ni, 30% Cu, 4% Si) przy użyciu technologii proszkowej ze względu na jego wartość technologiczną i ekonomiczną. Po przygotowaniu proszki krzemu, miedzi i niklu połączono w wyżej wymienionych proporcjach i rozdrobniono pod izostatycznym ciśnieniem na zimno (8 t). Próbki poddano laserowej obróbce powierzchniowej z odległości 100 cm z różną energią (0 mJ, 200 mJ, 260 mJ i 300 mJ) i czasem trwania impulsu (10 s). Badanie za pomocą dyfrakcji promieniowania rentgenowskiego wykazało, że wszystkie próbki mają strukturę sześciennie centrowaną (FCC). Warto zauważyć, że próbki poddane działaniu energii 300 mJ wykazywały najlepsze właściwości, w tym wzrost intensywności fazy. Obróbka laserowa stopiła wszystkie cząsteczki powierzchniowe, co poprawiło właściwości strukturalne. Twardość (mierzona metodą Rockwella), gęstość pozorna, absorpcja wody i porowatość uległy zmianie pod wpływem powierzchniowej obróbki laserowej. Próbki zanurzono również w 3,5-proc. roztworze NaCl na 3, 5, 7, 9 i 11 dni w celu zbadania wpływu obróbki cieplnej na odporność stopu na korozję. Parametry twardości wzrosły, podczas gdy współczynnik porowatości i absorpcja wody zmniejszyły się po obróbce laserowej. Stwierdzono również, że odporność na zużycie wzrasta wraz ze stopniem obróbki laserowej.

Słowa kluczowe: obróbka laserowa, XRD, stop Monel, technologia proszkowa

1. Introduction

S-Monel alloys are based on Ni-rich Ni-Cu alloys, typically containing around 30 wt% copper and 4 wt% silicon [1]. Monel was discovered in 1901 by Robert Crooks Stanley, who worked for the International Nickel Company (INCO) [2].

These alloys exhibit exceptional corrosion resistance in various environments, including seawater, acidic and alkaline media, as

Received / Otrzymano: 25.06.2024. Accepted / Przyjęto: 30.07.2024

Table 1. Purity and grain size for metallic powder
Tabela 1. Czystość i wielkość ziarna proszku metalicznego

Powder	Grain size [nm]	Purity [%]	Origin
Nickel powder	85	99.96	Fluka Chemie AG, Switzerland
Copper powder	95	99.95	Merck, Germany
Silicon powder	90	99.98	Fluka Chemie AG, Switzerland

Table 2. Alloy designations
Tabela 2. Oznaczenia stopu

Alloy	Laser energy [mJ]
A	0
B	200
C	260
D	300

Fig. 1. Grid on a balance
Rys. 1. Siatka na wadze

well as numerous oxidizing and reducing gas conditions [3]. They are also more durable than steel, with a low coefficient of thermal expansion and excellent resistance to alkalis. The International Nickel Company of Canada pioneered the industrial use of Monel alloys for vessels, pipelines, and valves, and they have since found applications in a wide range of sectors, from massive naval leviathans to small electronic components [4].

In addition to the primary components nickel (Ni) and copper (Cu), various minor elements are present in Monel alloys. For instance, H-Monel and S-Monel contain 3% and 4% silicon, respectively [5]. These alloys typically exhibit a face-centered cubic (FCC) structure in a single phase. Secondary alloying elements such as iron (Fe) and manganese (Mn) are also used and sourced from raw materials, and they contribute positively to corrosion resistance.

However, it is important to note that compositions in industrial standards can vary throughout the range, and composition control relies on empirical standards set by suppliers and end users [6, 7].

Ni, Cu, and Si exhibit negligible atomic size variations, which contribute to a uniform and homogeneous pressing process [8]. We developed a robust model of the S-Monel alloy based on these fundamental assumptions. Consequently, this study investigates the microstructural, physical, and mechanical properties of Monel alloys produced using powder metallurgy [9, 10].

2. Preparation of alloys

The alloy (Ni–Cu–Si) is composed of high-quality components, with an Fe and Ni content of at least 99.95%. Table 1 presents the grain sizes of metallic powders. These powders were blended to fabricate a Ni–Cu–Si alloy with a percentage of 66% Ni, 30% Cu, and 4% Si. Table 2 illustrates the alloy's characteristics under various energies (0 mJ, 200 mJ, 260 mJ, and 300 mJ). Subsequently, the powders were compressed under cold pressure at 8 t in a steel mold to produce cylindrical samples measuring 10 mm in diameter and 3 mm in thickness. These samples underwent laser surface treatment using a pulsed Nd:YAG laser with varying energy levels (0 mJ, 200 mJ, 260 mJ, and 300 mJ), a wavelength of 1064 nm, a pulse duration of 10 s, which was positioned at a distance of 100 cm.

3. Experimental

3.1. X-ray diffraction

The crystal structure of the produced alloys was analyzed using X-ray diffraction (XRD-6000) at angle (2θ = 40–80°) following Bragg's rule [11]:

$$2d \sin\theta = n\lambda, \tag{1}$$

where d represents the distance between two parallel levels, θ is the diffraction angle, and λ is the wavelength for X-rays. The following equation was utilized to calculate the crystal lattice constant a:

$$a = \sqrt{d^2 \cdot (h^2 + k^2 + l^2)}, \tag{2}$$

where h, k, l are the Miller indices.

A computer program was also used to verify that all Miller indices and phases measured at the diffraction angle were in accordance with the American Standard for Testing Materials (ASTM).

3.2. Microhardness

The Rockwell hardness test (HRC) was carried out on prepared samples in accordance with the British Standard [12, 13]. Microscopic hardness was evaluated by taking five measurements to indicate the uniformity and absence of defects on the surface. The arithmetic mean hardness value was calculated in units of gm/mm^2 to illustrate the visual correlation between hardness and surface laser treatment.

3.3. Apparent density, porosity, water absorption

The Archimedes technique was used to determine apparent density, porosity and water absorption after drying the samples for one hour in an electric drying oven at 100°C. The weight of the sample after removal from the oven is called the dry weight (W_d). The model was then immersed in a pot of water for 24 h. After extraction from the water, any water droplets on the surface were removed with a cotton cloth. Care had to be taken not to apply pressure to the model, as this could remove the water in its outer pores. Afterwards, the model was weighed, this weight being the saturated weight (W_s). The weight of the model was measured in a suspended state using a simple technique shown in Fig. 1. The water-soaked model was placed on a grid to be weighed and suspended in water, the weight being the hanging weight (W_i).

The apparent density (AD) was determined using the calculations below [14]:

$$AD = \frac{W_d}{W_d - W_i} \times \rho. \tag{3}$$

The apparent porosity (AP) is determined utilizing the following mathematical expression [15], wherein ρ denotes the density of water (1 g/cm^3):

$$AP = \frac{W_S - W_d}{W_S - W_i} \times 100\%, \tag{4}$$

where W_s signifies the weight of the model when saturated with water [gm], W_d denotes the weight of the model after

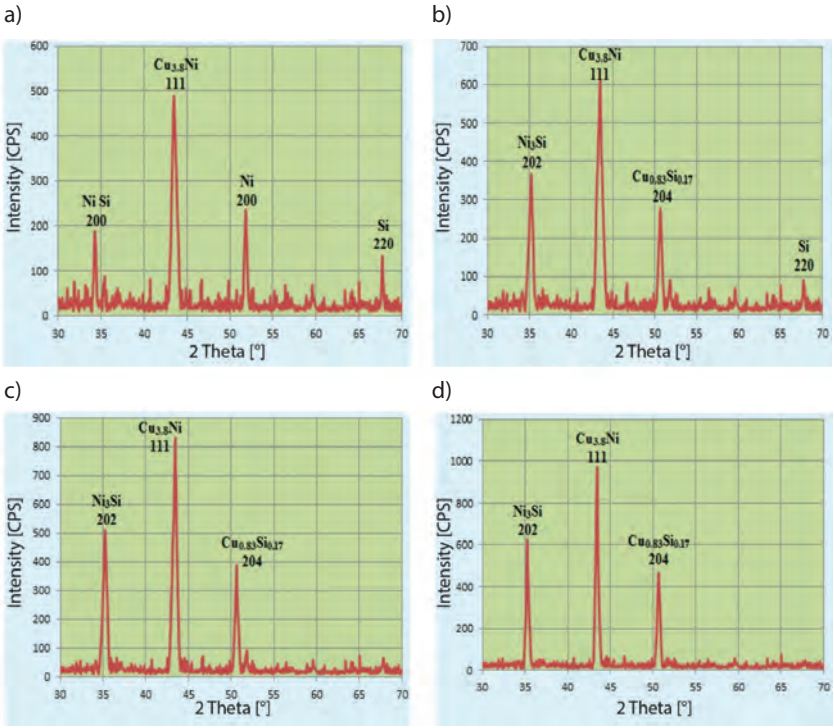

Fig. 2. X-ray diffraction: a) sample A , b) sample B, c) sample C, d) sample D

Rys. 2. Dyfrakcja rentgenowska: a) próbka A, b) próbka B, c) próbka C, d) próbka D

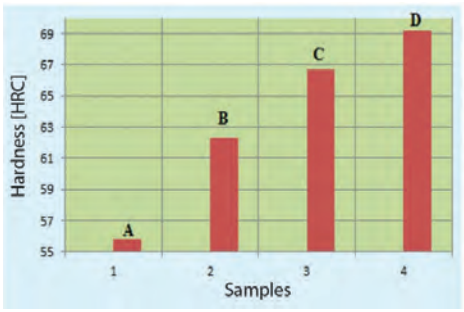

Fig. 3. Change in hardness values of samples

Rys. 3. Zmiana wartości twardości próbek

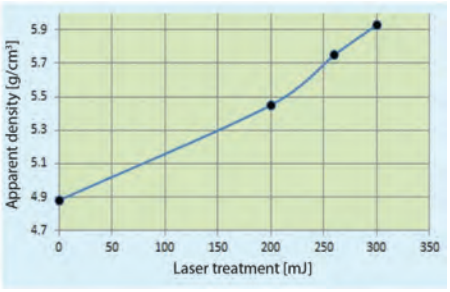

Fig. 4. Change of apparent density with laser treatment

Rys. 4. Zmiana gęstości pozornej po obróbce laserowej

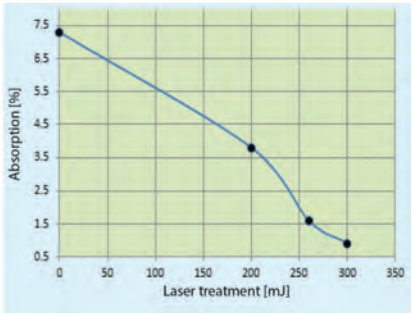

Fig. 5. Change of absorption with laser treatment

Rys. 5. Zmiana absorpcji po obróbce laserowej

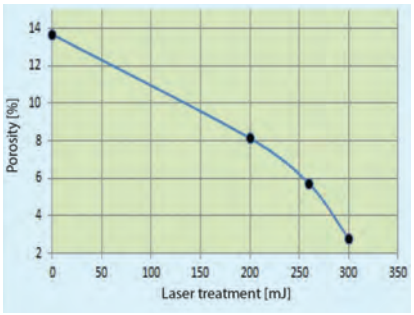

Fig. 6. Change of porosity with laser treatment

Rys. 6. Zmiana porowatości po obróbce laserowej

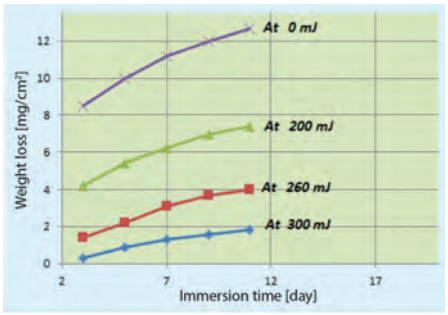

Fig. 7. Change of weight loss with immersion time

Rys. 7. Zmiana utraty masy wraz z czasem zanurzenia

drying [gm], and W_i indicates the weight of the model after suspension [gm].

The water absorption ratio (*WA*) was computed using the following equation [16]:

$$WA = \frac{W_S - W_d}{W_d} \times 100\%. \quad (5)$$

3.4. Corrosion average

After preparing the samples, the average corrosion was determined following their cleaning and polishing. The samples were weighed using a balance (Optika Level SR 6532, Italy) and immersed in a 3.5% NaCl solution for different durations (3, 5, 7, 9, and 11 days) before being removed, dried, and reweighed. The amount of weight loss was calculated using the following equation [17]:

$$W = \frac{M_g - W_i}{A} \quad \left[\frac{\text{mg}}{\text{cm}^2}\right], \quad (6)$$

where M_g represents the mass of the sample block before it is immersed in the erosion medium, W_i represents the mass of the sample block after immersion, and *A* represents the surface area of the sample [cm^2].

4. Results and discussion

Fig. 2–5 display the diffraction peaks of the samples, indicating that all samples possess an identical atomic structure resembling a face-centered cube. The Miller (*h*, *k*, *l*) indices of the diffraction peaks exhibit either even or odd values, which aligns with the findings from previous investigations [18–20].

It is important to mention that the $Cu_{3.8}Ni$ phase appears in all numbers. Furthermore, the laser treatment resulted in the identification of two distinct phases: Ni_3Cu and $Cu_{0.83}Si_{0.17}$. The laser surface energy is elevated by intensifying the three phases ($Cu_{3.8}Ni$, Ni_3Cu, $Cu_{0.83}Si_{0.17}$) due to the enhancement of crystal growth and improved uniformity of the crystal structure with pressure removal and porosity reduction [21, 22].

On the other hand, it was observed that hardness values increased in proportion to the extent of the surface laser treatment. This illustrates the uniform and homogeneous distribution

of crystalline structures following laser treatment, as well as the melting of surface particles, resulting in an enhancement of the alloy's composition (Fig. 3).

Fig. 4. indicates that the apparent density values of the samples rose in proportion to the extent of the surface laser treatment employed in the investigation, leading to a reduction in voids and enhanced alloy homogeneity. This observation aligns with the findings reported in the study [10, 23].

Fig. 5 and 6 illustrate the porosity and water absorption values for the examined samples. These data suggest that an increase in laser treatment results in decreased water absorption and porosity. As laser treatment enhances bonding between powder granules, there is a scarcity of pores and a change in form. This decrease in both porosity and absorption levels indicates a correlation between them, inversely linked to apparent density [24, 25].

Fig. 7 illustrates the notable weight loss observed with increased immersion duration for all laser sessions. This indicates a decrease in the metal's corrosion resistance with longer immersion times [26–28].

5. Conclusions

1. The XRD analysis unveiled the crystalline structure of the samples as face-centered cubic (FCC).
2. Elevated laser energy results in heightened diffraction peak intensity, indicative of crystal growth and structural uniformity.
3. Increased laser treatment leads to higher apparent density and hardness.
4. Increasing laser treatment corresponds to reduced porosity ratio and water absorption rates.
5. The study revealed that increasing laser therapy enhances corrosion resistance.

CRediT authorship contribution statement
Omar Fadhil Abdullah: Formal analysis.
Orass Abdulhadi Hussein: Software.
Marwan Al-Lattouf: Writing – original draft.
Salih Y. Darweesh: Conceptualization, Data curation, Methodology.

BIBLIOGRAPHY

[1] Q. Li, Y. B. Xu, Z. H. Lai, L. T. Shen, Y. L. Bai. 2000. "Dynamic Recrystallization Induced by Plastic Deformation at High Strain Rate in a Monel Alloy." *Materials Science and Engineering: A* 276(1–2): 250–256. DOI: 10.1016/S0921-5093(99)00127-6.

[2] B. Li, J. Gu, Q. Wang, C. Ji, Y. Wang, J. Qiang, C. Don. 2012. "Cluster Formula of Fe-Containing Monel Alloys with High Corrosion-Resistance." *Materials Characterization* 68: 94–101. DOI: 10.1016/j.matchar.2012.04.002.

[3] Y. Yang, C. Wei, Y. Yao, X. Chen, W. Li, Y. Jia, Z. Chen, J. Hu. 2023. "Explosive Cladding of Monel Alloy Tube and Copper Rod." *International Journal of Mechanical Sciences* 247: 108173. DOI: 10.1016/j.ijmecsci.2023.108173.

[4] O. F. Abdullah, O. A. Hussein, E. T. Karash. 2020. "The Laser Surface Treatment Effective on Structural Properties for Invar Alloy (Fe–Ni) Type Prepared by Powder Technology." *Key Engineering Materials* 844: 97–103. DOI: 10.4028/www.scientific.net/kem.844.97.

[5] K. D. Ramkumar, V. Joshi, S. Pandit, M. Agrawal, O. S. Kumar, S. Periwal, M. Manikandan, N. Arivazhagan. 2014. "Investigations on the Microstructure and Mechanical Properties of Multi-Pass Pulsed Current Gas Tungsten Arc Weldments of Monel 400 and Hastelloy C276." *Materials and Design* 64: 775–782. DOI: 10.1016/j.matdes.2014.08.055.

[6] J. Chen, J. Wang,, F. Yan, Q. Zhang, Q. Li. 2015. "Effect of Applied Potential on the Tribocorrosion Behaviors of Monel K500 Alloy in Artificial Seawater." *Tribology International* 81: 1–8. DOI: 10.1016/j.triboint.2014.07.014.

[7] U. Esgin, D. Özyürek, H. Kaya. 2016. "An Investigation of Wear Behaviors of Different Monel Alloys Produced by Powder Metallurgy." *AIP Conference Proceedings* 1727: 020008. DOI: 10.1063/1.4945963.

[8] Z. Wang, L. Fang, I. Cotton, R. Freer. 2015. "Ni–Cu Interdiffusion and Its Implication for Ageing in Ni-Coated Cu Conductors". *Materials Science and Engineering: B* 198: 86–94. DOI: 10.1016/j.mseb.2015.04.006.

[9] R. Monzen, Y. Shimada, C. Watanabe. 2010. "Mechanical Properties of Cu–Ni–Be System Alloys." *Journal of Physics Conference Series* 240(1): 4. DOI: 10.1088/1742-6596/240/1/012102.

[10] A. Varea, E. Pellicer, S. Pané, B. J. Nelson, S. Suriñach, M. Dolors Baró, J. Sort. 2012. "Mechanical Properties and Corrosion Behaviour of Nanostructured Cu-Rich CuNi Electrodeposited Films." *International Journal of Electrochemical Science* 7(2): 1288–1302. DOI: 10.1016/S1452-3981(23)13414-6.

[11] C. Kittel. 2005. *Introduction to Solid State Physics*. Hoboken, New Jersey: John Wiley and Sons.

[12] M. Zhang, Y. Wu, H. Cui, J. Cheng.2021. "Research on the Relationship between Solid Physics and Quantum Mechanics Based on Computer." *Journal of Physics: Conference Series* 1744: 032176. DOI: 10.1088/1742-6596/1744/3/032176.

[13] O. F. Abdullah, A. K. Jarallah, F. Maher, R. R. Yahia. 2022. "A Synthetic Study of Archaeological (Cu–Sn–P) Bronze Alloy Maintenance by Simulation Method." *AIP Conference Proceedings* 2394: 020001. DOI: 10.1063/5.0120926.

[14] I. K. Jassim , K. H. Erzaich, O. F. Abdullah, M. A. Majeed. 2015. "The Effect of Heat Treatment on the Physical and Mechanical Properties of the (Alnico-5) Alloy Prepared by Powder Metallurgy Method." *Advanced in Applied Science Research* 6(8): 36–41. DOI: 10.13140/RG.2.2.23934.23361.

[15] Y. Kocak. 2010. "A Study on The Effect of Fly Ash and Silica Fume Substituted Cement Paste and Mortars." *Scientific Research and Essays* 5(9): 990–998.

[16] L. A. Dobrzański, B. Dołżańska. 2010. "Structure and Properties of Sintered Tool Gradient Materials." *Journal of Achievements in Materials and Manufacturing Engineering* 43(2): 711–733.

[17] E. J. Salih, S. M. A. Allah, S. Y. Darweesh, H. A. Mohammed. 2021. "Study of Some of the Physical Variables of a Metal-Based System Using the Powder Method." *Journal of Physics: Conference Series* 1999(1): 012068. DOI: 10.1088/1742-6596/1999/1/012068.

[18] N. A. Ghazal, Z. N. Majeed, S. Y. Darweesh. 2024. "The Effect of Adding Different Percentages Manganese on Some Mechanical and Magnetic Properties of Composite (Al–Cu)." *AIP Conference Proceedings* 2885: 040003. DOI: 10.1063/5.0182248.

[19] E. J. Salih, S. M. A. Allah, S. Y. Darweesh. 2022. "Study the Structural and Mechanical Properties of the Cu–WC Composite." *AIP Conference Proceedings* 2398: 020035. DOI: 10.1063/5.0094030.

[20] A. T. Dahham, T. Q. Jassim, S. Y. Darweesh. 2023. "Study the Effect of Adding Nano-Magnesium Oxide on Some Structural and Mechanical Properties of (Cu–10% Fe)." *AIP Conference Proceedings* 2977: 040031. DOI: 10.1063/5.0182510.

[21] A. S. Karim, Z. N. Majeed, S. Y. Darweesh. 2021. "The Effect of Nanostructured Zirconia Reinforcement on the Mechanical and Structural Properties of a Copper-Based System." *Materials Science Forum* 1039: 297–306. DOI: 10.4028/www.scientific.net/MSF.1039.297.

[22] M. S. Hamoudi, A. S. Mahmoud, S. Y. Darweesh. 2022. "Studying the Effect of Grinding Time on the Physical and Mechanical Properties of the Ternary System (Al–Ni–MgO) by Powder Method." *NeuroQuantology* 20(3): 626–635. DOI: 10.14704/nq.2022.20.3.NQ22351.

[23] S. H. Hameedi. 2021. "Study Effect Treatment Thermal for Cermet Composite Prepared by Flame Thermal Spray Method." *Kirkuk Journal of Science* 15(4): 42–55. DOI: 10.32894/kujss.2021.167517.

[24] H. H. Ahmed, A. R. Ahmed, S. Y. Darweesh, Z. T. Khodair, M. A. Al-Jubbori. 2020. "Processing of Turbine Blades Using Cermet Composite Materials." *Journal of Failure Analysis and Prevention* 20: 2111–2118. DOI: 10.1007/s11668-020-01027-0.

[25] S. Y. Darweesh, I. K. Jassim, A. S. Mahmood. 2019. "Characterization of Cerment Composite Coating Al_2O_3–Ni System." *Journal of Physics: Conference Series* 1294(2): 022011. DOI: 10.1088/1742-6596/1294/2/022011.

[26] A. M. Ibraheem, S. M. A. Allah, S. Y. Darweesh. 2021. "Enhancement the Properties of Aluminum by Adding Boron Carbide by the Powder Method." *Journal of Physics: Conference Series* 1999: 012074. DOI: 10.1088/1742-6596/1999/1/012074.

[27] S. H. Humeedi, S. M. Abdulkareem, S. Y. Darweesh. 2022. "The Synthetic and Mechanical Properties of a Silica Matrix Cermet Composite." *Journal of Wuhan University of Technology: Materials Science* 37(3): 423–428. DOI: 10.1007/s11595-022-2548-5.

[28] M. N. Ahmed, N. A. Daham, S. Y. Darweesh. 2024. "Structural and Mechanical Properties for (Ni–WC) System by Using Thermal Spray." *AIP Conference Proceedings* 2885: 020013. DOI: 10.1063/5.0181722.